RESEARCH PAPER

Preparation of Nanocomposite Heteropoly Metalate Based Graphene Oxide: Insight into Cadmium Adsorption

Hanieh Fakhri[1], *Ali Reza Mahjoub*[1,*], *Hassan Aghayan*[2]

[1] *Department of Chemistry, Tarbiat Modares University, Tehran, Iran*

[2] *Nuclear science and Technology Institute, , Tehran, Iran*

ARTICLE INFO

Article History:
Received 07 May 2017
Accepted 15 June 2017
Published 01 July 2017

Keywords:
Cadmium
Graphene oxide
Heteropoly metalate
Nanocomposite

ABSTRACT

We developed a facile strategy for preparation of heteropoly metalate/graphene oxide nanocomposite as a new ion exchanger for cadmium ion removal from aqueous solution. The synthesized nanocomposite was characterized by X-ray powder diffraction (XRD), UV-Vis spectroscopy, FT-IR spectroscopy and Raman spectroscopy. Our findings indicated that the combination of heteropoly metalate nanoparticles with graphene oxide results in an excellent performance for cadmium ions removal of aqueous solution. The experimental data demonstrated that the adsorption isotherm fitted well by Langmuir model with maximum sorption capacity of 47.85 mg/g. The removal behavior of this compound was evaluated by various parameters such as contact time, concentration of metal ion, pH of solution and temperature. In addition, the effect of interfering cations on the cadmium adsorption is investigated. Dubinin–Radushkevich model represented physical sorption occurred as bold mechanism that is confirmed by thermodynamic parameters. Also, the obtained data of the recycling experiment presented excellent stability after 4 consecutive cycles. This study indicated heteropoly metalate supported graphene oxide with good performance for removal of cadmium can be used for treating polluted solution by other heavy metal.

How to cite this article
Fakhri H, Mahjoub A. R, Aghayan H. Preparation of Nanocomposite Heteropoly Metalate Based Graphene Oxide: Insight into Cadmium Adsorption. J Nanostruct, 2017; 7(3):223-235. DOI: 10.22052/jns.2017.03.009

INTRODUCTION

Water contamination by heavy metals has become a serious subject of worldwide concerns. Discharge of these heavy metals from various sources like mining, Ni–Cd batteries, oil refineries, smelting operations and pigments quickly are increasing in the recent years [1]. So, the removal of these toxic pollutions from aqueous waste is nowadays considered as a hot issues being investigated. Cadmium (Cd) as a component of heavy metals group attracted notable attention due to high toxicity, tendency to accumulation in liver and kidney [2], non-biodegradable and also has bad effects on ecosystem [3,4]. The World Health Organization (WHO) is considered cadmium as one of the most dangerous heavy metals and a drastic human carcinogen [5]. Several methods such as chemical precipitation, reverse osmosis and solvent extraction [6, 7] are employed for treatment of polluted solution. However, these methods are unsuitable due to incomplete removal of the heavy metal and so additional treatment is required. Other methods such as ultrafiltration and electrochemical deposition are used in developed industrial but high cost and complexity of process limited their

* *Corresponding Author Email: mahjouba@modares.ac.ir*

usage [8]. Many of research studies is introduced ion exchange as an effective method for treating contaminated solution, particularly ion exchange process by inorganic materials that have in nurture ion exchange properties like heteropoly acids (HPAs). HPAs nanoparticles are made of particular combination of hydrogen and oxygen with certain metals and non-metals. Nowadays, Keggin structure of HPAs (with overall formula $[XM_{12}O_{40}]^{n-}$, where X is the heteroatom (eg P^{5+}, Si^{4+}, or B^{3+}) and M is the addenda atom (most common are molybdenum and tungsten)) is attracted more attention in this area. Potential acidic properties is one of the excellent properties of keggin structure that it enable as ion exchanger to remove metals ion [9,10]. This ability comes back to the interaction of metal ions in solution with an oxygen end-atom and a release of exchangeable protons in the HPAs structure. So they can act as cation- exchange materials. However, low surface area and high solubility in aqueous media limited its usage as ion exchanger. The formation of salt of these compounds leads to increase their surface area and insolubility in aqueous solution. Siddiqui et al. reported the synthesis of Zirconium (IV) tungsto iodo phosphate and used it for the separation of Pb^{2+} from other metal ions [11]. Mittal et al. synthesized zirconium antimono phosphate and zirconium phosphor tungstate as inorganic ion exchanger and reported that these have good ion exchange capacity for Fe^{2+}, Fe^{3+}, Pb^{2+} and Ba^{2+}[12]. However, their separation and filtration even under conditions of high speed centrifugation still is confined their practical applications. Recently, many researches focused on fabrication of nanocomposite by inserting the nanoparticles on the various supports such as silica [13], multi walled carbon [14] and carbon nanotubes [15] that is an important study for the exploration of their properties and applications. Graphene oxide (Go) with layer structure is the most attractive and the newest member of carbon family that has various functional groups such as carboxyl, hydroxyl and epoxy. Layer structure and also presence of different functional groups introduced it as desirable support. Composites of decorated Go sheets by nanoparticles with oxidative and acidic properties such as HPAs are developed [16, 17]. As an evident point from the literature, the immobilization of HPAs on the graphene based surfaces produces new nanocomposite materials which have potential importance in the areas such as optics, electronics, catalysis and sensors [18-20]. Anyway, there is a little evaluation of heteropoly metalate supported graphene oxide. In the present study, tin (IV) molybdo tangsto phosphate, donated as TMTP, supported Go was prepared via a simple strategy and in the first time, its application for removal of Cd ions was studied. Finally adsorption experiments directed to examine effective parameters such as metal ion concentration, pH of solution, temperature and presence of alkaline metal ions.

MATERIALS AND METHODS

Materials

All of the materials were used in this research work purchased from Merck and Aldrich without further purification.

Characterization

FT-IR analyses of materials were performed using a Shimadzu-8400S spectrometer in the range of 400-4000 cm^{-1}. The crystalline structure of products were recorded by powder X-ray diffraction (XRD) on philips X-pert X-ray diffractometer using Cu Kα radiation (wavelength, λ = 1.5418 ˚A). The morphology of various samples was obtained with scanning electron microscopy (SEM, Philips XL-300 instrument). Inductively Coupled Plasma (ICP, Varian vista-PRO) was employed to evaluate the cadmium value. The Raman spectra of samples were recorded by the Almega Thermo Nicolet Dispersive Raman Spectrometer (Laser second harmonic @532 nm of a Nd: YLF laser). UV-Vis spectra were achieved with Shimadzu-UV-2550-8030 spectrophotometer in the range of 200-800 nm at room temperature.

Preparation of H_3 $[PMo_4W_8O_{40}]$ particles

HPAs with general formula $H_3[PMo_4W_8O_{40}].nH_2O$, were synthesized via the procedure of Huixiong [21]. Briefly, Na_2HPO_4 (2.23 gr) and desired amount of sodium molybdate were dissolved in distilled water. So, the solution was stirred at 90 ˚C. After being stirred for 30 min, aqueous solution of $Na_2WO_4.2H_2O$ was added to the above heated solution. Subsequently, aqueous sulfuric acid solution was added dropwise until the solution pH value reached 1.5–2. In the following, the mixture was heated at 90 ˚C and then final product was extracted by diethyl ether and following was recrystallized. ICP analysis indicated that the atomic ratio of P/Mo/W were: 1/ 3.86/ 7.69 that

this product, 4-molybdo-8-tangsto phosphoric acid, is symbolized as MTP.

Preparation of TMTP/Go composites

Go was prepared by a modified procedure according to the literature [22]. TMTP supported Go, donated as TMTP/Go, was synthesized as follows: First, 1gr Go was dispersed in 40 ml water. So 3 gr MTP added to it and was stirred at 300 ˚C until the solvent was completely volatilized. Subsequently, the collected precipitate was calcined at 300 ˚C for 3 h. Acidic solution of $SnCl_4$. $5H_2O$ (0.31 gr $SnCl_4 \cdot 5H_2O$ dissolved in 10 ml HCl) was added to above precipitate and was stirred at the room temperature. The sample was filtered and washed with distilled water and ethanol and dried in an oven at 60 ˚C for 18 h. ICP elemental analysis indicated that 20% of TMTP species was loaded on the Go support that indicated as 20%TMTP/Go. This procedure was used for preparation of other loading of TMTP on the support.

Adsorption experiment

Batch technique was employed to determine the adsorption capacities of Cd ions. For this purpose, 0.1 gr of adsorbent was mixed in a 20 mL of preselected concentration of metal ion solution. The mixture was continuously shaken by the mechanical shaker at 150 rpm and 25 ºC. The desired pH of the solution was adjusted using negligible volumes of 0.1 M nitric acid and sodium hydroxide solution. At the end of adsorption experiments, the solid phase was collected by centrifuged at 6000 rpm for 10 min and the residual concentration of Cd in aqueous solution was determined by ICP-OES elemental analysis. Also the effect of different conditions such as pH, contact time, concentration of metal ions and temperature of solutions on adsorption efficiency were investigated. In order to examine influence of interfering cations containing Ca^{2+} and Mg^{2+} on adsorption process, Cd solution with initial concentration 200 ppm was added to various concentration of interfering cations (80, 160 and 240 ppm). The equilibrium adsorption capacity was calculated according to Eq. 1

$$qe = \frac{(Co - Ce)v}{W} \quad (1)$$

where C_0 and C_e are the initial and equilibrium concentration of the metal ions (mg. L^{-1}), v is the volume of the liquid phase (ml) and W is the mass of the adsorbent (gr).

RESULTS AND DISCUSSION

Adsorbent characterization

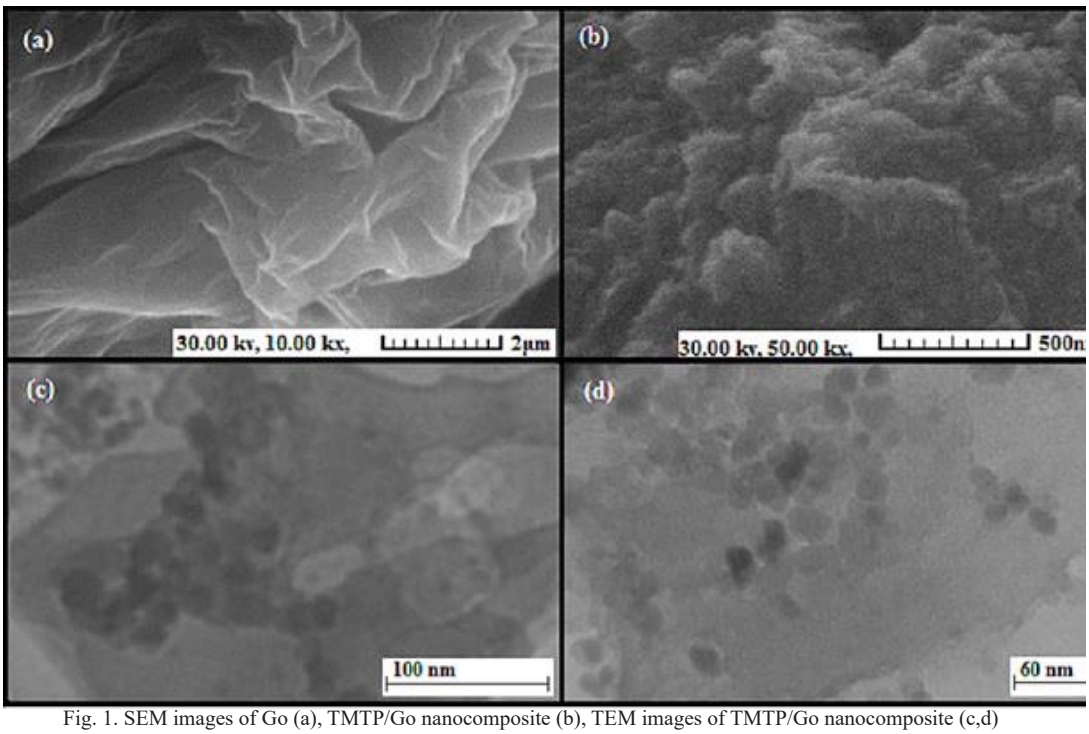

Fig. 1. SEM images of Go (a), TMTP/Go nanocomposite (b), TEM images of TMTP/Go nanocomposite (c,d)

The morphology and texture of produced samples were investigated by SEM and TEM analysis. As seen in Fig.1a, the smooth and silk-like sheets were observed for Go sample. It is found from Fig.1b and TEM images in Fig. 1c , d that surfaces of supports (Go) were randomly covered by lots of TMTP nanoparticles which suggesting a strong interaction between TMTP nanoparticles and Go. The purity phase of synthesized products examined with XRD analyses as shown in Fig. 2. The diffraction peak at 2θ= 8.9˚ correspond to the (001) reflection of Go (Fig. 2a) [23]. As shown in fig. 2b, XRD patterns of MTP sample are in good agreement with its reported patterns in previous study indicating phase purity and good crystalline of it [21]. In the long-range ordered XRD pattern of TMTP/Go (Fig. 2c) the absence of any diffraction peaks related to TMTP in composite diagram implies the high dispersion of TMTP on the Go support [24]. The FT-IR spectrum of Go (Fig. 3a) indicated peaks at 1056 cm-^{1}, 1226 cm^{-1}, 1622 cm^{-1} and 1732 cm^{-1} that correspond to alkoxy C–OH stretching vibrations, epoxy C–O–C stretching vibrations, aromatic C═C stretching vibrations and C = O stretching vibrations of the -COOH groups, respectively [25]. The broad peak corresponded to the hydroxyl groups and the adsorbed water on surface is located at 3381 cm^{-1} [26]. Fig. 3b showed four characteristic peaks belonging to MTP at 1051 cm^{-1}(ν_{P-O}), 951 cm^{-1}($\nu_{m=o}$), 877 cm^{-1} ($\nu_{Mo-O-Mo}$) and 741 cm^{-1} ($\nu_{Mo-O-Mo}$) [21]. FT-IR spectra of TMTP/Go demonstrated that the structure of TMTP is remained in composition sample (Fig. 3c) and confirmed the presence of both Go and TMTP in the nanocomposite. TMTP interact with functional groups such as carbonyl, carboxyl and other group of Go. Especially, in aqueous solution the carboxyl group is weakly acidic but when it is bonded with TMTP that have a lower pH value; it alters to a weak base by changing to a positive charge. So, electrostatic bonding between positively charged carboxyl groups and negatively charged TMTP anions improved interaction TMTP with surface of Go [27]. In comparing between the Go and TMTP/Go spectra, red shift of C=O peak was observed from 955 cm^{-1} to 941 cm^{-1} that this may be referred to electrostatic bonding between TMTP and Go. UV-Vis spectroscopy was applied to evaluate the ligand-to-metal charge transfer (LMCT) band of the pure MTP in 200-800 nm regions. The adsorption edge MTP was measured using the first derivative of the absorption spectrum. The calculated band gap (Fig. 4a) in the case of the pure MTP is 2.25 eV (edge wavelength 551 nm). This value shifted to 2.88 eV for TMTP/Go sample. This shift in the band gap clearly associated with the changed energy levels of MTP owing to electron transfer from MTP to Go [28]. These results were supported by

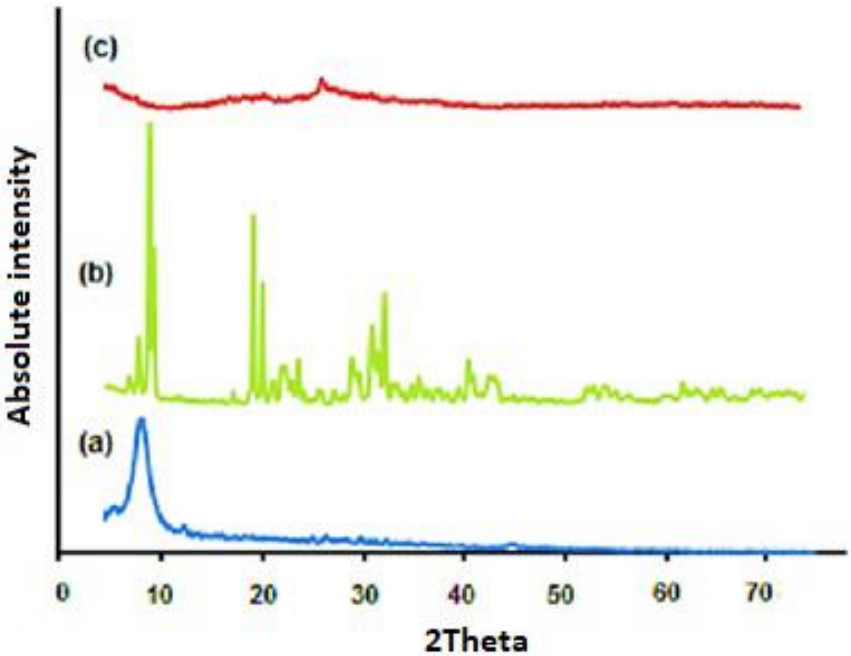

Fig. 2. XRD pattern of Go (a), MTP (b) and TMTP/Go (c) nanocomposite

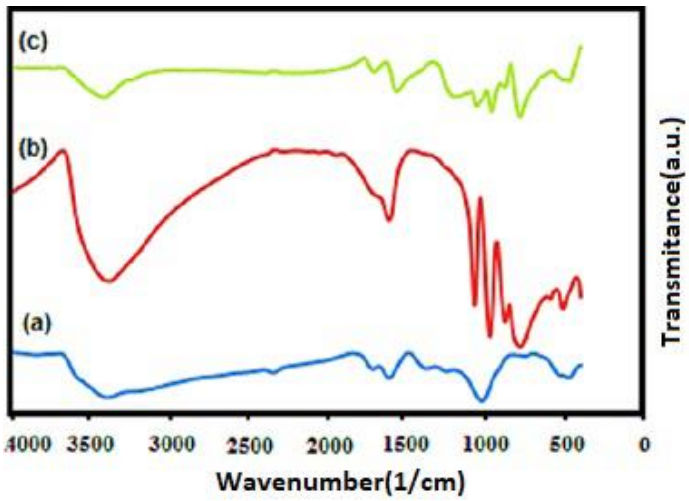

Fig. 3. FT-IR spectra of Go (a), MTP (b) and TMTP/Go (b) nanocomposite

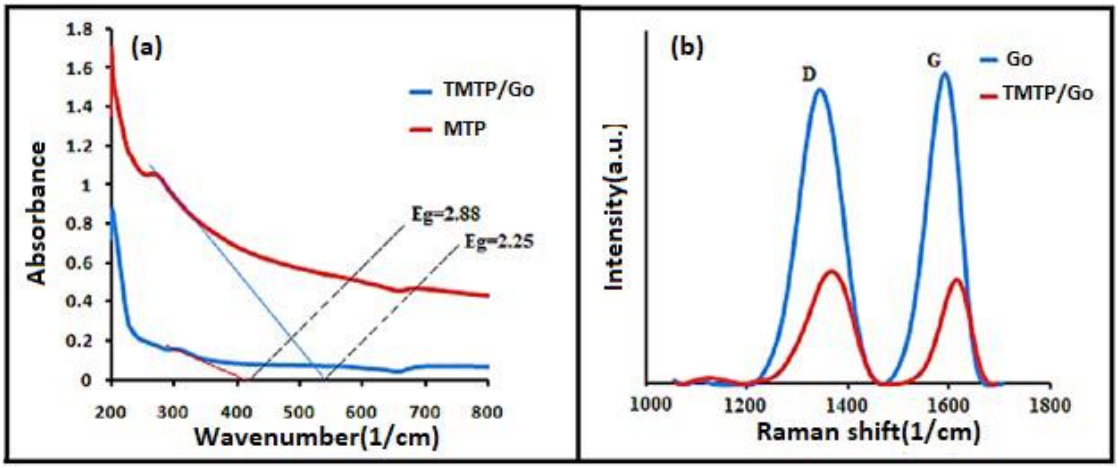

Fig. 4. UV-Vis spectra of MTP and TMTP/Go nanocomposite (a), Raman spectra of Go and TMTP/Go nanocomposite (b)

Raman spectroscopy. Interaction between Go and TMTP can be investigated by the changes of the degree of disorder in crystalline structure carbon materials using Raman spectroscopy. The Raman spectrum of Go exhibited two peaks at 1360 cm^{-1} and 1650 cm^{-1} which are attributed to existing disorder in the carbon structure (D band) and E_2g mode of sp^2 bonds of carbon framework (G band) respectively. The obtained I_D/I_G ratio for Go and TMTP/Go are 0.94, 1.04 respectively (Fig. 4b). The increased ratio indicated the anchoring of TMTP onto Go resulted in increased defect of the sp^2 domain which can be assumed as a good evidence for successful formation TMTP/Go.

Adsorption tests

Effect of amount of loading on removal efficiency

The dependence of Cd^{2+} removal to the presence of TMTP /Go composite shown in Fig. 5. It is clear that only 27% of Cd^{+2} removed by pure Go. When TMTP/Go is used as adsorbent, removal efficiency was enhanced with the increase of loading amount. The efficiency reaches the maximum when the TMTP loading increase up to 30%. The fall of removal efficiency with the further increasing of loading was corresponded to aggregation of TMTP species on surface of TMTP/Go composite.

Effect of pH solution

The initial pH of solution plays important role in determining adsorption nature of adsorbent. The different cadmium species exist in aqueous solution such as Cd^{+2}, $Cd(OH)^+$, $Cd(II)(OH)_2$, $Cd(OH)_2(s)$, $[Cd(OH)_3]^-$and $[Cd(OH)_4]^{2-}$ that

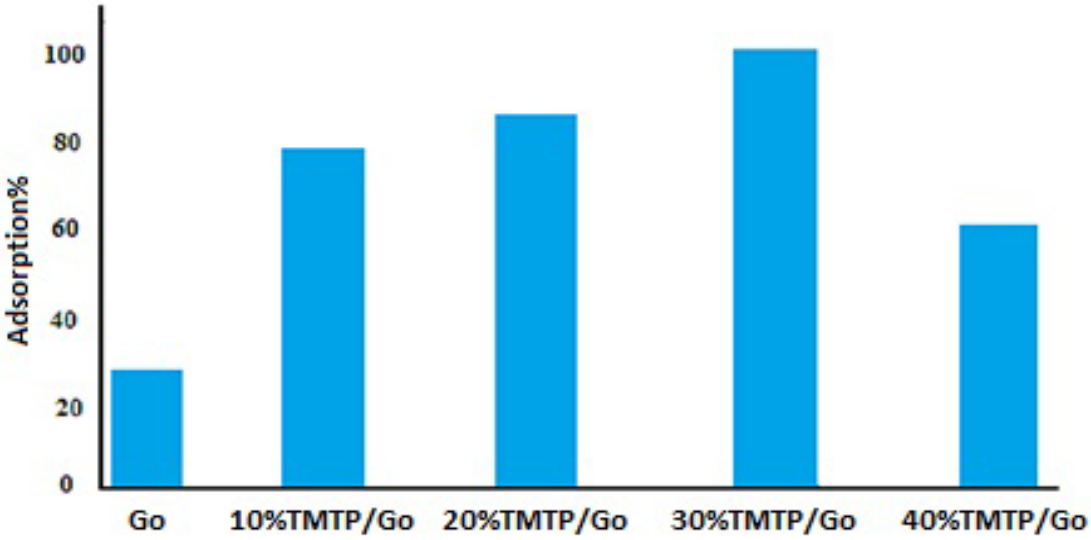

Fig. 5. Removal efficiency of Go and TMTP/Go nanocomposite by various loading of MTP

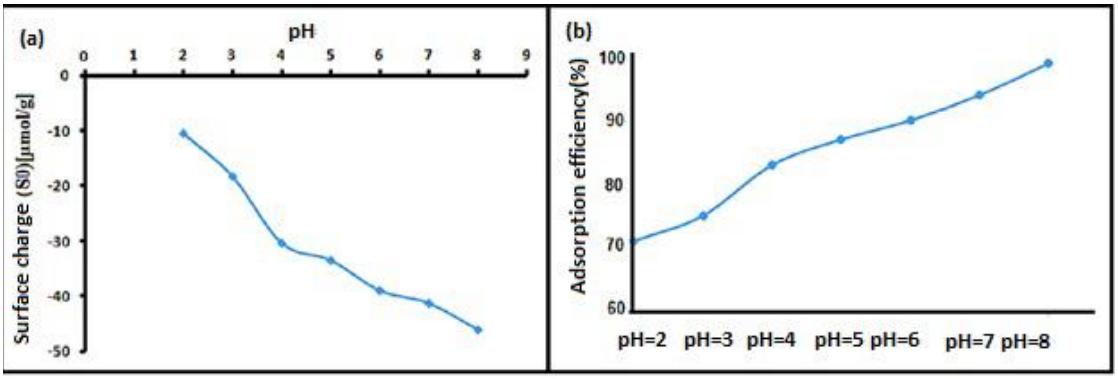

Fig. 6. The surface charge versus pH for 30%TMTP/Go nanocomposite (a), The effect of pH solution on the Cd2+ removal efficiency (b)

concentration of each of them depends on pH of solution. Cd^{+2} is dominant species at pH 8 [29]. Hence, the considered value range of pH is adjusted between 2-8. Results of Zeta potential for 30%TMTP/Go nanocomposite demonstrated in Fig. 6a. It is seen, this nanocomposite is negatively charged at the entire mentioned range pH (2pH8). As shown in Fig. 6b, the removal of metal ion increases along with increasing the pH from 2 until 8. In the lower values of pH, competition of Cd^{2+} ions with H^+ or H_3O^+ for adsorption on negative surface adsorbent increase and so decrease of Cd removal is expected. For a higher pH, it is seen that adsorption efficiency is reached to maximum value at pH=8 that attributed to decline of protons concentration resulting enhancement of Cd^{2+} removal.

Effect of contact time

In particular, adsorption kinetics is important character for fast treatment water. The adsorption of Cd^{+2} from aqueous solution at initial concentration of 10 ppm on the adsorbent as a function of contact time is represented in Fig. 7a. As shown, the adsorption process is rapid within the first 60 min and reached equilibrium within 180 min. The initial rapid adsorption can be ascribed to expanded access to active sites due to plane layer structure of Go unlike other supports such as SBA-15 or carbon nanotube that lead easy migrate of Cd^{+2} ions to the external active site of TMTP/Go nanocomposite and Subsequently, the slow diffusion rate of Cd^{+2} ions into the internal site of adsorbent.

In the present work, three models of kinetic reaction including pseudo-first-order, pseudo-

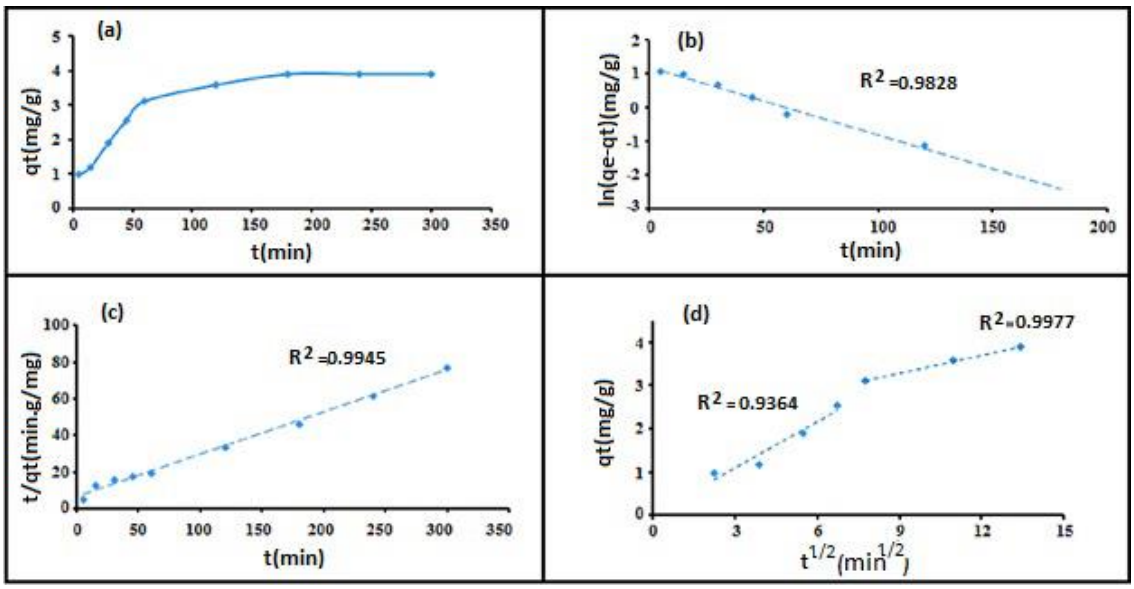

Fig. 7. Adsorption kinetic of 30%TMPT/Go composite (a), pseudo-first-order linear plot (b), pseudo-second-order linear plot (c), Intraparticle diffusion kinetic plot for adsorption Cd2+ ion (d)

second-order and intraparticle diffusion model were used to test the fitness of the experimental data and evolution of the adsorption rate of Cd^{+2} ions in various steps. The linearized forms of these semi-empirical kinetic models relation are shown as follow, respectively [30, 31];

$$\log(q_e - q_t) = log q_e - \frac{k_1}{2.303} \quad (2)$$

$$\frac{t}{q_t} = \frac{1}{k_2 q_e^2} + \frac{1}{q_e} t \quad (3)$$

$$q_t = k_d t^{1/2} + c \quad (4)$$

Where q_e (mg/g) and q_t (mg/g) are the sorption amounts per unit mass at equilibrium and at time t; k_1 is the pseudo-first-order rate constant, k_2 is pseudo-second-order rate constant, k_d is diffusion rate constant and c is the intercept that corresponded to the thickness of the boundary layer. The fitting parameters and the correlation factors (R^2) of the pseudo-first-order and pseudo-second-order kinetic models are depicted in Fig. 7b, c and Table 1. The high correlation factor and good accordance between the experimental q_e value and calculated value of pseudo-second-order kinetic model indicated that the adsorption dynamics obey pseudo-second-order model (R^2= 0.9945).

For the better identify of diffusion mechanism, the Weber–Morris intraparticle diffusion model

Table 1. kinetic adsorption parameters of pseudo-first-order and pseudo-second-order models

Concentration (mg. L^{-1})		Pseudo-first-order				Pseudo-second-order	
	q_e^{Exp}(mg/g)	K_1 (1/min)	q_{e1} (mg/g)	R^2	K_2 (g/mg min)	q_{e2} (mg/g)	R^2
10	3.89	0.2	3.4	0.9828	$7.8*10^{-3}$	4.35	0.9945

Table 2. Intraparticle diffusion parameters for Cd2+ adsorption by 30%TMPT/Go nanocomposite

Concentration (mg.L^{-1})	Stirring rate(rpm)	K_d (mg/g.$min^{1/2}$)	C (mg/g)	R^2
10	150	0.1398	2.026	0.9977

was then used [32]. This model can be ascribed the mass transfer steps in the Cd^{+2} ions adsorption onto adsorbent. The plots of q_t versus $t^{1/2}$ (Fig. 7d) in the range of the studied adsorption give nonlinear curve and did not pass through the origin (C≠0) that described intraparticle diffusion was not the only rate-controlling step. The initial portion can be assigned to the boundary layer diffusion (film diffusion) and the second portion with lower slop reflected to the slow adsorption step where the intraparticle diffusion is involved in adsorption process but not the only rate controlling step (fig. 7d, Table 2). The initial portion with larger slop has a faster rate than second portion. This rapid rate is due to the significant availability to active adsorption sites on sheets of Go and on the other hand, the lower slope of second portion resulted a low adsorption rate owing to decreased concentration of ion is spent long time to diffuse.

Effect of the initial metal ion concentration

Fig. 8 shows the adsorption isotherm of Cd^{+2} ions by 30%TMTP/Go nanocomposite at the initial concentration range of 10-200 mg. L^{-1}. Adsorption isotherm can represent the significant parameters for designing a favorable adsorption system. The isotherm data were simulated to the Langmiur (Fig. 8b), Freundlich (Fig. 8c) and Dubinin–Radushkevich (D-R) models (Fig. 8d).

The obtained parameters of these models can be employed to evaluation of surface properties and affinity of the adsorbent toward metal ions. The Langmuir model assumes that metal ions are adsorbed as monolayer coverage without any interaction between adsorbed species [33]. The linear form of this model is shown in the following relation;

$$\frac{C_e}{q_e} = \frac{1}{bQ_0} + \frac{C_e}{Q_0} \tag{5}$$

where Q_0 (mg. g^{-1}) is the required amount of metal to form a monolayer and b (L. mg^{-1}) is the constant that referred to energy of adsorption. The equilibrium parameter or separation factor (R_L) is other important parameters that obtained of Langmuir plot by the following equation;

$$R_L = \frac{1}{1 + bC_0} \tag{6}$$

where C_0 (mg. L^{-1}) is the highest initial concentration in the solution. The R_L reflect the type of isotherm to be favorable ($0 < R_L < 1$) or unfavorable ($R_L > 1$).

The Freundlich model assumes multilayer adsorption onto heterogeneous surface [34]. The linearized form of this equation is represented as;

$$logq_e = logk_f + \frac{1}{n} logc_e \tag{7}$$

where k_f is the Freundlich constant related to the multilayer adsorption of the adsorbent and n is linearity index related to the adsorption intensity.

The Dubinin–Radushkevich (D–R) isotherm

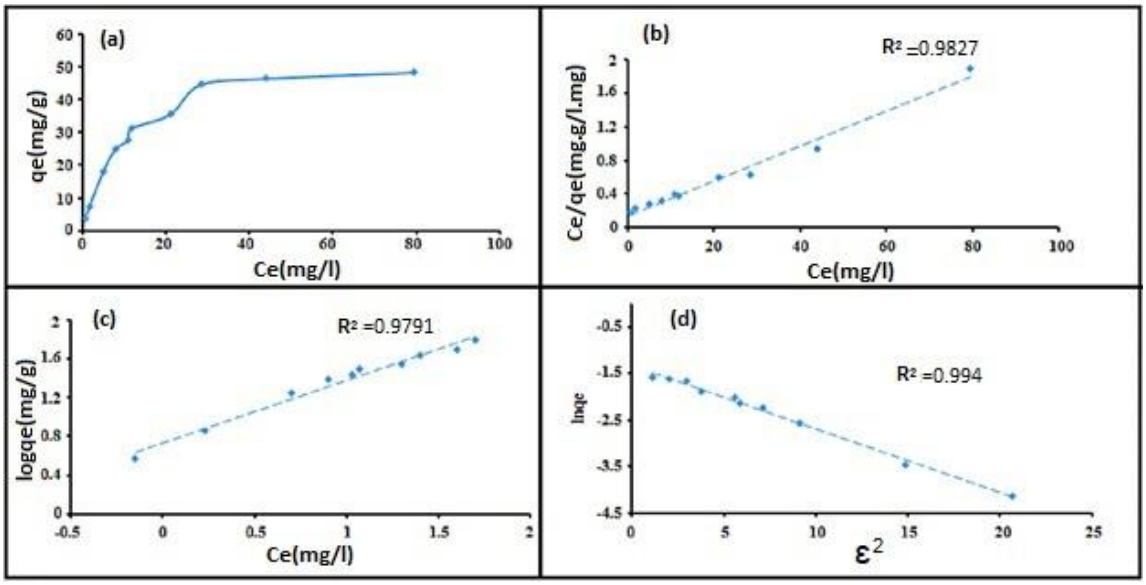

Fig. 8. Adsorption isotherm of 30%TMPT/Go composite (a), linear Langmuir plot (b) linear Freundlich plot (c), linear Dubin- Radushkevich plot (d)

Table 3. Langmuir and Freundlich parameters for adsorption of Cd2+ by 30%TMPT/Go nanocomposite

Metal ion	Langmuir				Freundlich		
	Q_m(mg/g)	b (l/mg)	R^2	R_L	K_f	n	R^2
Cd	47.85	0.14	0.98	0.42	5.45	1.54	0.97

Table 4. The Dubin- Radushkevich parameters for adsorption of Cd2+ by 30%TMPT/Go nanocomposite

C_0(mg. L^{-1})	T(K)	E(kJ. mol^{-1})	R^2
10	297	1.9	0.994

model is usually applied to determine the type sorption process (chemical or physical sorption) which were expressed in the following equation;

$$ln(q_e) = lnq_{DR} - B_{DR}\varepsilon^2 \quad (8)$$

where q_{DR} is the monolayer capacity (mmol. g^{-1}), B_{DR} (mol^2. J^{-2}) is referred to adsorption energy and ε is the Polanyi potential which is calculated by;

$$\varepsilon = RTln\left(1 + \frac{1}{C_e}\right) \quad (9)$$

where R is the gas universal constant (8.314 J. $mol.^{-1}$ K^{-1}) and T is the absolute temperature (K). The value of E (kJ. mol^{-1}) is mainly parameters of (D–R) equation for estimation the type of sorption process. This parameter can be obtained according to the below equation [34]:

$$E = \frac{1}{\sqrt{2B_{DR}}} \quad (10)$$

If value of E was less than 8 kJ. mol^{-1}, the physical sorption mainly will occur and if value of E was 8-16 kJ. mol^{-1} the chemical sorption will be expected. The fitted results investigated in this work are tabulated in Table 3 and 4.

As can be seen in Table 3, The sorption isotherm of Cd^{+2} could be fitted better by Langmuir than Freundlich model with high correlation coefficient values (R^2 > 0.98) that is described Cd^{+2} ion is adsorbed as a monolayer coverage onto specific sites of 30%TMTP/Go composite. Also, q_m of this composite measured from the Langmuir isotherm is 47.85 mg/g. It can be seen from Table 3, the value of R_L is 0.42, implied favorable adsorption as it places in 0 to 1 range. It is also seen, the value of n (1.54) is lied between 1 and 10, resulted that the sorption is favorable under desired condition.

The values of E were between 1 and 8 (Table 4) indicating that physical attraction can be affected on Cd^{+2} ions sorption. Table 5 revealed some adsorption capacity by different adsorbents that reported previously. As can be seen, TMTP/Go nanocomposite with desirable adsorption capacity has excellent adsorption performance.

Adsorption thermodynamics

The relations among temperature and Cd^{2+} ions adsorption described by the following formulas:

$$\Delta G^\circ = \Delta H^\circ - T\Delta S^\circ \quad (11)$$

$$lnKc = \frac{\Delta S^\circ}{R} - \frac{\Delta H^\circ}{RT} \quad (12)$$

where the ΔG° is the change in Gibbs free energy

Table 5. Comparison of adsorption capacity of Cd2+ by various adsorbent

Adsorbent	Q_m(mg/g)	Reference
Oak wood char	0.37	[36]
Dodecylamine-41A	41.59	[37]
SH-HMS	14.61	[38]
Buffalo weed biochar	11.63	[39]
Dairy manure biochar	32.03	[40]
Rice straw biochar	34.13	[41]
Activated silica gel Modified with 1,2-ethylenediamine	19.60	[42]
Chrysotile nanotubes	39.23	[43]
tetraethoxy orthosilan xerogel	35.71	[44]
IpomoeaBiochar	41.67–72.43	[45]
30%TMT/Go composite	47.85	This study

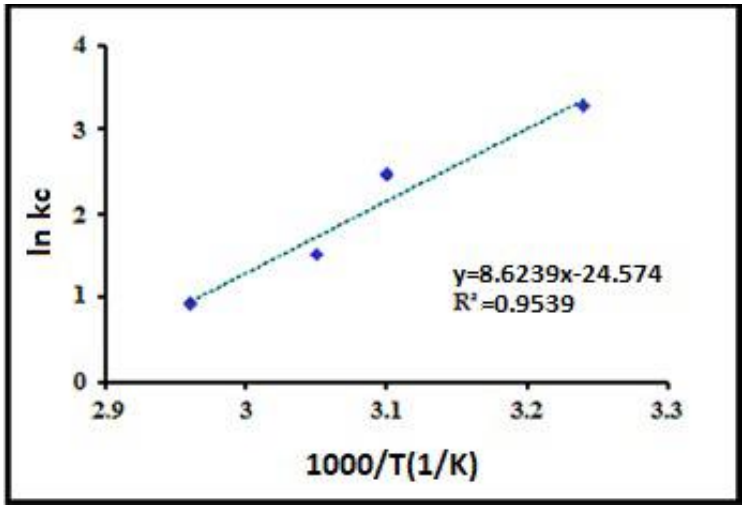

Fig. 9. The plot of lnkC versus 1/T, the effect of temperature on adsorption of Cd^{2+} ion

Table 6. Thermodynamic parameters for Cd^{2+} adsorption in various temperatures

C_0(mg. L^{-1})	T(K)	ΔG^0 (kJ.mol^{-1})	ΔH^0 (kJ.mol^{-1})	ΔS^0 (J.k^{-1}.mol^{-1})	R^2
	308	-8.76			
10	318	-6.72	-71.69	-204.30	0.9539
	328	-4.68			
	338	-2.63			

(J. mol^{-1}), the values of ΔH˚ is the change in the enthalpy (J. mol^{-1}) and ΔS˚ is the change in the entropy (J. $mol.^{-1}$ K^{-1}). The equilibrium constant (k_c) is determined from the metal ion concentration in the adsorbent (C_a) and the solution (C_e) respectively.

$$K_c = \frac{C_a}{C_e} \quad (13)$$

The effect of temperature on the adsorption of Cd^{+2} is indicated in Fig. 9 by linear plot of ln k_c vs. 1/T. As can be seen in Table 6, the negative ΔG˚ at all temperature demonstrate spontaneously nature of this adsorption process and exothermic behavior suggested by obtained negative value of ΔH˚ for this process.

Generally, if 0<ΔG<-20 KJ/mol, physical adsorption is dominant and it changes to more negative values than -40 KJ/mol for chemical adsorption [46]. The obtained ΔG˚ in all temperatures are between 0 and -20 KJ/mol that referred to physical adsorption and in accordance with gained result of Dubinin–Radushkevich model. The negative values of ΔS˚ represented decreased randomness in solid/solution interface that maybe implies the liberation of two H^+ along with Cd^{+2} ions adsorption on adsorbent and following capturing of H^+ by various functional groups on the surface of adsorbent.

Effect of Ca^{2+} and Mg^{2+}

The effect of Ca^{2+} and Mg^{2+} cations on adsorption process as interfering cations is investigated. Adsorption capacity is decreased to 43.89 and 44.92 mg/g with presence 80 ppm of Ca^{2+} and Mg^{2+} ions (initial concentration of Cd^{2+} fixed at 200 ppm). The reduction of adsorption capacity is reached to 34.28 and 37.18 mg/g when concentration of interfering cations is 240 ppm. As observed in Fig. 10, the inhibiting impact of Ca^{2+} is greater than Mg^{2+}. The greater effect of Ca^{2+} on Cd^{2+} adsorption is because of more similar ion radii of Ca^{2+} with Cd^{2+} than Mg^{2+} (ion radius are 0.99, 0.97 and 0.65 ˚A for Ca^{2+} with Cd^{2+} and Mg^{2+} respectively). On the other hand, Ca^{2+} can form complexes with water molecules, Ca^{2+}-$(H_2O)_n$, that covering surface of adsorbent which resulting decreased availability of active sites on the adsorbent. It can be expected, Ca^{2+}-$(H_2O)_n$ with larger radius than Mg^{2+}-$(H_2O)_n$ has

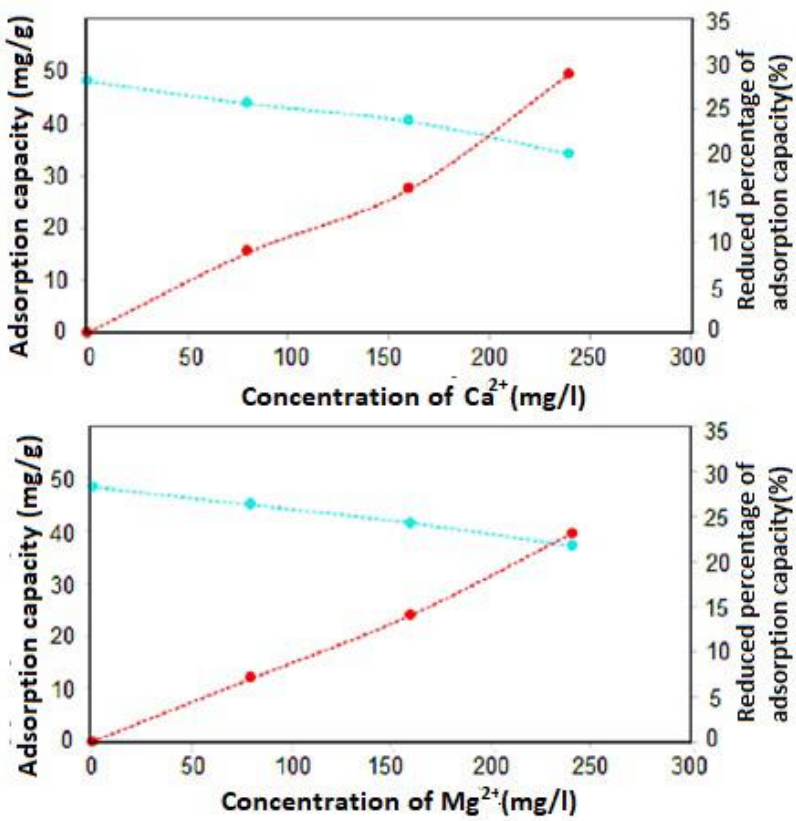

Fig. 10. The effect of interfering cations on adsorption efficiency

bigger steric hindrance and so its negative effect on adsorption is stronger [47]. Since concentration of Ca^{2+} and Mg^{2+} in fresh water is approximately between 10-80 ppm, so the presence of these cations with these levels of concentration have not significant effect on Cd^{2+} adsorption.

Reusability

Reusability is considered a particular parameter for evaluation the economy and applicability of

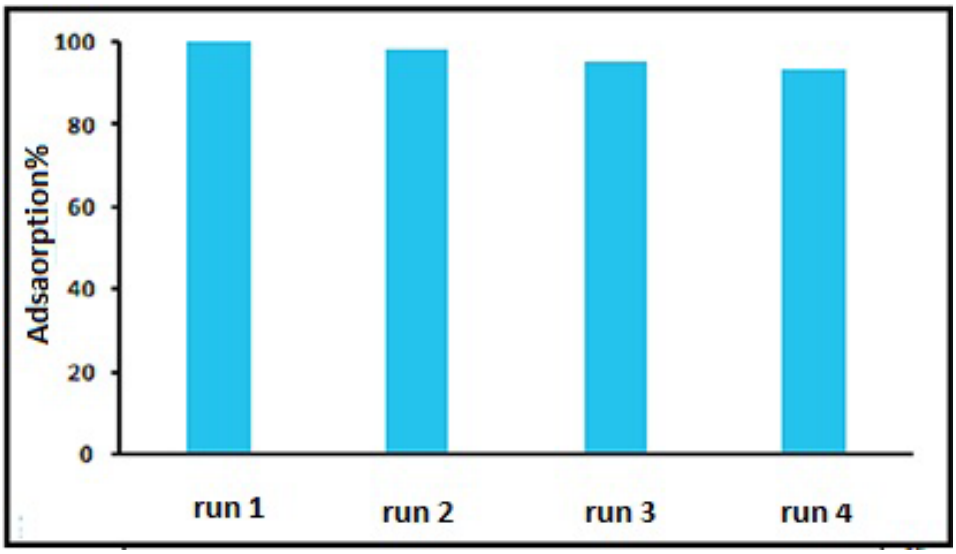

Fig. 11. Adsorbent recycled runs versus removal efficiency of Cd^{2+} ion

adsorbents. Desorption of Cd^{+2} was carried out by desorbing solution containing water and 0.01M HCl. As seen in Fig. 11, adsorption efficiency slightly decreased from 100% to 93% after four cycles at the same condition indicating a good reusability of the adsorbent.

CONCLUSION

We have successfully synthesized a TMTP/Go nanocomposite through easy fabrication method in an aqueous solution. The electron transfer and electrostatic interaction proposed as two kind of interactions between Go and TMTP. The FT-IR, UV-Vis and Raman spectroscopy confirmed interaction between Go and TMTP. The enhanced removal of Cd^{+2} obtained by 30%TMTP/Go nanocomposite compared with pure Go. Isothermal data of Cd^{+2} adsorption on 30%TMTP/Go can be fitted by Langmuir isotherm and also, kinetic analysis can be described by pseudo-second-order model. Thermodynamic data demonstrated that the adsorption capacity decreased with increasing the temperature resulting the exothermic behavior of adsorption process. This ability to remove Cd^{+2} ions metal from solution indicates the high potential of TMTP/Go nanocomposite for cleaning the environment and industrial waste effluents from heavy metal ions and this preparation procedure can be considered for synthesis of the other salt of heteropoly metalate/Go nanocomposite.

ACKNOWLEDGMENT

The financial support of this study by Tarbiat Modares University is gratefully acknowledged.

CONFLICT OF INTEREST

The authors declare that there are no conflicts of interest regarding the publication of this manuscript.

REFERENCES

1. Ebadi1 M, Shagholani H, Jahangiri H. High Efficient Nanocomposite for Removal of Heavy Metals (Hg2+ and Pb2+) from Aqueous Solution. J. Nanostruct. 2016; 6(1): 23-27.
2. Sun X, Liu X, Yang B, Xu L, Yu S. Functionalized chrysotile nanotubes with mercapto groups and their Pb(II) and Cd(II) adsorption properties in aqueous solution. J. Mol. Liq. 2015; 208: 347–355.
3. Bian Y, Bian Z, Zhang J, Ding A, Liu S, Zheng L, Wang H. Adsorption of Cadmium Ions from Aqueous Solutions by Activated Carbon with Oxygen-containing Functional Groups. Chin. J. Chem. Eng. 2015; 23: 1705-1711.
4. Nordberg G.F. Historical perspectives on cadmium toxicology. Toxicol. Appl. Pharm. 2009; 238: 192–200.
5. WHO. Guidelines for Drinking Water Quality, Vol 1: Recommendations, 2nd ed. WHO: Geneva, 1993.
6. Ricci B. C, Ferreira C. D, Aguiar A. O, Amaral M.C.S. Integration of nanofiltration and reverse osmosis for metal separation and sulfuric acid recovery from gold mining effluent. Sep. Purif. Technol. 2015; 154: 11–21.
7. Daryabor M, Ahmadi A, Zilouei H. Solvent extraction of cadmium and zinc from sulphate solutions: Comparison of mechanical agitation and ultrasonic irradiation. Ultrason Sonochem. 2017; 34: 931–937.
8. Ahmad-Zaini M.A, Okayama R, Machida M. Adsorption of aqueous metal ions on cattle-manurecompost based activated carbons. J. Hazard. Mater. 2009; 170: 1119–1124
9. Mittal S. K, Singh P, Sharma H.K. New development of inorganic ion exchanger: synthesis of new zirconium based ion exchangers and their characterization. JSIE. 2005; 16: 76-82.
10. Garvey G.B.M, Moffat J.B. Ion-exchange properties of microporous monovalent salts of 12-tungstophosphoric acid and 12-molybdophosphoric acid catalysts. J. Catal. 1991; 128: 69-83.
11. Siddiqui W. A, and Khan S. A. Synthesis, characterization and ion exchange properties of zirconium (IV) tungstoiodophosphate, a new cation exchanger. Bull. Mater. Sci. 2007; 30: 43-49.
12. Mittal S. K, Singh P, and Kumar Sharma H. Synthesis of new Zirconium based ion exchangers and their characterization. J Ion Exchange. 2005; 16: 76-82.
13. Grinenval E, Rozanska X, Baudouin A, Berrier E, Delbecq F, Sautet P, Basset J, Lefebvre F. Controlled Interactions between Anhydrous Keggin-Type Heteropolyacids and Silica Support: Preparation and Characterization of Well-Defined Silica – Supported Polyoxometalate Species. J. Phys. Chem. C. 2010; 114: 19024–19034.
14. Xia X, Fan D, An B, Cai Y, Wei Q. Electrochemical behavior of Keggin-type heteropolyanion doped composite of polyaniline and multi-walled carbon nanotubes., J. Mol. Liq., 2015, 206, 335–337.
15. Kawasaki N, Wang H, Nakanishi R, Hamanaka S, Kitaura R, Shinohara H, Yokoyama T, Yoshikawa H, Awaga K. Nanohybridization of Polyoxometalate Clusters and Single-Wall Carbon Nanotubes: Applications in Molecular Cluster Batteries. Angew. Chem. Int. Ed. 2011; 50: 3471–3474.
16. Guo W, Tong X, Liu S. Polyoxometalate/chitosan–electrochemically reduced graphene oxideas effective mediating systems for electrocatalytic reduction of persulfate. Electrochim Acta. 2015; 173: 540–550.
17. Yang M.H, Kim D.S, Lee T. J, Lee S.J, Lee K.G, Choi B.G. Polyoxometalate-grafted graphene nanohybrid for electrochemical detection of hydrogen peroxide and glucose. J. Colloid Interface Sci. 2016; 468: 51–56.
18. Chen J, Liu S, Feng W, Zhanga G, and Yang F. Fabrication

phosphomolybdic acid–reduced graphene oxide nanocomposite by UV photo-reduction and its electrochemical properties. Phys. Chem. 2013; 15: 5664-5669.

19. Liu R, Li S, Yu X, Zhang G, Zhang S, Yao J, Keita B, Nadjo L, and Zhi L. Facile Synthesis of Au-Nanoparticle/Polyoxometalate/ Graphene Tricomponent Nanohybrids: An Enzyme-Free Electrochemical Biosensor for Hydrogen Peroxide. Small. 2012; 8: 1398–1406.
20. Liu R, Li S, Yu X, Zhang G, Zhang S, Yaoc J, and Zhi L. A general green strategy for fabricating metal nanoparticles/ polyoxometalate/graphene tri-component nanohybrids: enhanced electrocatalytic properties. J. Mater. Chem. 2012; 22: 3319–3322.
21. Huixiong W, Mei Z, Yixin Q, Haixia L, Hengbo Y. Preparation and Characterization of Tungsten-substituted Molybdophosphoric Acids and Catalytic Cyclodehydration of 1,4-Butanediol to Tetrahydrofuran. Chin. J. Chem. Eng. 2009; 17: 200-206
22. William H, Offeman R.E. Preparation of Graphitic Oxide. J. Amer. Chem. Soc. 1958; 80:1339-1339.
23. Fakhri H, Mahjoub A.R, CheshmeKhavar A.H. Improvement of visible light photocatalytic activity over graphene oxide/CuInS2/ ZnO nanocomposite synthesized by hydrothermal method. Mater. Sci. Semicond. Process. 2016; 41: 38–44.
24. Fumin Z, Chaoshu Y, Jun W, Yan K, Haiyang Z, Chunyan W. Synthesis of fructone over dealmuinated USY supported heteropoly acid and its salt catalysts. Journal of Molecular Catalysis A. 2006; 247: 130-137.
25. Basheer C. Application of titanium dioxide-graphene composite material for photocatalytic degradation of alkylphenols. J. Chem. 2013; 2013: 1–10.
26. Tan L.L, Ong W.J, Chai S.P, Mohamed A.R. Reduced graphene oxide-TiO2 composite as a promising visible-light-active photocatalyst for the conversion of carbon dioxide. Nanoscale Res. Lett. 2013; 8: 465–473.
27. Kim Y, Shanmugam S. Polyoxometalate−Reduced Graphene Oxide Hybrid Catalyst: Synthesis, Structure, and Electrochemical Properties. ACS Appl. Mater. Interfaces. 2013; 5: 12197–12204.
28. Tessonnier J.P, Goubert-Renaudin S, Alia S, Yan Y, and Barteau M.A. Structure, Stability, and Electronic Interactions of Polyoxometalates on Functionalized Graphene Sheets. Langmuir. 2013; 29: 393–402.
29. Bian Y, Bian Z.Y, Zhang J. X, Ding A. Z, Liu S. L, Wang H. Effect of the oxygen-containing functional group of graphene oxide on the aqueous cadmium ions removal. Appl surf sci. 2015; 329: 269-275.
30. Ho Y. Review of second-order models for adsorption systems. J Hazard Mater B. 2006; 136: 681-689.
31. Lagergren S. Zur theorie der sogenannten adsorption gel¨oster stoffe. Handlingar. 1898; 24: 1-39.
32. Weber W.J, Morris J.C. Kinetics of adsorption on carbon from solution. J. Sanit. Eng. Div. Am. Soc. Civ. Eng. 1963; 89: 31-60.
33. Langmuir I. The adsorption of gases on plane surfaces of glass, mica and platinum. JACS. 1918; 40: 1361–1403.
34. Gunten U.V. Ozonation of drinking water: Part I. Oxidation kinetics and product formation. Water Res. 2003; 37: 1443–1467.
35. Dubinin M.M. The potential theory of adsorption of gases and vapors for adsorbents with energetically non-uniform surface. Chem. Rev. 1960; 60: 235–266.
36. Mohan D, Pittman C.U, Bricka M, Smith F, Yancey B, Mohammad J, Steele P.H, Alexandre-Franco M.F, Gomez-Serrano V, Gong H. Sorption of arsenic, cadmium, and lead by chars produced from fast pyrolysis of wood andbark during bio-oil production. J. Colloids Interface Sci. 2007; 310: 57–73.
37. Benhamou A, Baudub M, Derrichea Basly, J.P. Aqueous heavy metals removal on amine-functionalized Si-MCM-41 and Si-MCM-48. J Hazard Mater. 2009; 171: 1001–1008.
38. Machida M, Fotoohi B, Amamo Y, Ohba T, Kanohd H, Mercier L. Cadmium (II) adsorption using functional mesoporous silica and activated carbon. J Hazard Mater. 2012; 221–222: 220–227.
39. Yakkala K, Yu M.R, Roh H, Yang J.K, Chang Y.Y. Buffalo weed (Ambrosiatrifida L. var. trifida) biochar for cadmium (II) and lead (II) adsorption in singleand mixed system. Desalin, Water Treat. 2013; 51: 7732–7745.
40. Xu X, Cao X, Zhao L, Wang H, Yu H, Gao B, Removal of Cu, Zn, and Cd from aqueous solutions by the dairy manure-derived biochar. Environ. Sci. Pollut. Res. 2013; 20; 358–368.
41. Han X, Liang C.F, Li T.Q, Wang K, Huang H.G, Yang X.E. Simultaneous removal of cadmium and sulfamethoxazole from aqueous solution by ricestraw biochar. J. Zhejiang Univ. Sci. B. 2013; 14: 640–649.
42. Kushwaha A.K, Chattopadhyaya M.C. Surface modification of silica gel for adsorptive removal of Ni2+ and Cd 2 + from water. Desalin Water Treatm. 2015; 54: 1642–1650.
43. Sun X, Liu X, Yang B, Xu L, Yu S. Functionalized chrysotile nanotubes with mercapto groups and their Pb(II) and Cd(II) adsorption properties in aqueous solution. J. Mol. Liq. 2015; 208: 347–355.
44. Saranda F.B, Hassania S, Fazlia M, Haghbeen K. Nanoporous Xerogel for Adsorption of Pb2+ and Cd2+. J. Nano Struct. 2015; 5: 209-218.
45. Goswami R, Shim J, Deka S, Kumari D, Kataki R, Kumar M. Characterization of cadmium removal from aqueous solution by biochar produced from Ipomoea fistulosa at different pyrolytic temperatures. Ecological Engineering. 2016; 97: 444–451.
46. Liu X, Luo J, Zhu Y, Yang Y, Yang S. Removal of methylene blue from aqueous solutions by an adsorbent based on metal-organic framework and polyoxometalate. J. Alloys Compd. 2015; 648: 986-993.
47. Cheng C, Wanga J, Yanga X, Lia A, Philippe C. Adsorption of Ni(II) and Cd(II) from water by novel chelating sponge and the effect of alkali-earth metal ions on the adsorption. J Hazard Mater. 2014; 264: 332– 341.